Eur. Phys. J. C 22, 255–267 (2001)
Digital Object Identifier (DOI) 10.1007/s100520100814

THE EUROPEAN PHYSICAL JOURNAL C

A study of $\Sigma^{\pm}$, $\Sigma^{*\pm}$ and $\overline{\Sigma}^{-}_{1385}$ production in the hyperon beam experiment WA89 at CERN

The WA89 Collaboration

M.I. Adamovich[8], Yu.A. Alexandrov[8,a], S.P. Baranov[8,a], D. Barberis[3], M. Beck[5], C. Bérat[4], W. Beusch[2], M. Boss[6], S. Brons[5,b], W. Brückner[5], M. Buénerd[4], Ch. Busch[6], Ch. Büscher[5], F. Charignon[4], J. Chauvin[4], E.A. Chudakov[6,c], U. Dersch[5], F. Dropmann[5], J. Engelfried[6,d], F. Faller[6,e], A. Fournier[4], S.G. Gerassimov[8,f], M. Godbersen[5], P. Grafström[2], Th. Haller[5], M. Heidrich[5], E. Hubbard[5], R.B. Hurst[3], K. Königsmann[5,g], I. Konorov[5,8,f], N. Keller[6], K. Martens[6,h], Ph. Martin[4], S. Masciocchi[5,i], R. Michaels[5,c], U. Müller[7], H. Neeb[5], D. Newbold[1], C. Newsom[j], S. Paul[5,f], J. Pochodzalla[5,k], I. Potashnikova[5], B. Povh[5], R, Ransome[l], Z. Ren[5], M. Rey-Campagnolle[4,m], G. Rosner[7], L. Rossi[3], H. Rudolph[7], C. Scheel[n], L. Schmitt[7,f], H.-W. Siebert[6], A. Simon[6,g], V. Smith[1,o], O. Thilmann[6], A. Trombini[5], E. Vesin[4], B. Volkemer[7], K. Vorwalter[5], Th. Walcher[7], G. Wälder[6], R. Werding[5], E. Wittmann[5], M.V. Zavertyaev[8,a]

[1] University of Bristol, Bristol, UK
[2] CERN, 1211 Genève 23, Switzerland
[3] Genoa Univ./INFN, Dipt. di Fisica, 16146 Genova, Italy
[4] Grenoble ISN, 38026 Grenoble, France
[5] Heidelberg Max-Planck-Inst. für Kernphysik, Postfach 103980, 69029 Heidelberg, Germany
[6] Universität Heidelberg, Physikalisches Institut, 69120 Heidelberg Germany[p]
[7] Universität Mainz, Inst. für Kernphysik, 55099 Mainz, Germany
[8] Moscow Lebedev Physics Inst., 117924, Moscow, Russia

Received: 4 February 2001 / Revised version: 25 June 2001 /
Published online: 12 November 2001 –

Abstract. We report on a measurement of the inclusive production cross sections for $\Sigma^{\pm}$, $\Sigma^{\pm}_{1385}$, $\Sigma^{\pm}_{1660}$ and $\overline{\Sigma}^{-}_{1385}$ in the CERN hyperon beam experiment WA89, using a Σ^{-}/π^{-} beam of 345 GeV/c momentum and neutrons of 260 GeV/c mean momentum. A strong leading particle effect was observed for all negative Σ and Σ^{*}. The results are compared with predictions from phenomenological models.

1 Introduction

The study of inclusive production of hadrons in hadron beams with a diversity of strangeness content in the beam projectiles and the produced particles can provide new insights into hadron interactions, since various degrees of valence quark overlap between incoming and outgoing hadrons can be isolated. The role of the valence quark overlap in the so-called "leading particle effect" has been known since a long time and has been clearly demonstrated in earlier hyperon beam experiments [1].

So far, even a coherent phenomenological model of hadroproduction is still lacking. The Lund model in the form of the PYTHIA and similar programs [2] predicts

[a] Supported by Deutsche Forschungsgemeinschaft, contract number DFG 436 RUS 113/465/0-2(R), and Russian Foundation for Basic Research under contract number RFFI 00-02-04018
[b] Now at TRIUMF, Vancouver, B.C., Canada V6T 2A3
[c] Now at Thomas Jefferson Lab, Newport News, VA 23606, USA
[d] Now at Instituto de Fisica,Universidad Autonoma de San Luis Potosi, S.L.P. 78240 Mexico
[e] Now at Fraunhofer Inst. für Solar Energiesysteme, 79100 Freiburg, Germany
[f] Now at Technische Universität München, Garching, Germany
[g] Now at Fakultät für Physik, Univ. Freiburg, Germany
[h] Now at Department of Physics and Astronomy, SUNY at Stony Brook, NY 11794-3800, USA
[i] Now at Max-Planck-Institut für Physik, München, Germany
[j] University of Iowa, Iowa City, IA 52242, USA
[k] Universitaät Mainz, Institut für Kernphysik, Germany
[l] Rutgers University,Piscataway, NJ 08854, USA
[m] *Permanent address:* CERN, 1211 Genève 23, Switzerland
[n] NIKEF, 1009 DB Amsterdam, The Netherlands
[o] Supported by the UK PPARC
[p] Supported by the Bundesministerium für Bildung, Wissenschaft, Forschung und Technologie, Germany, under contract numbers 05 5HD15I, 06 HD524I and 06 MZ5265

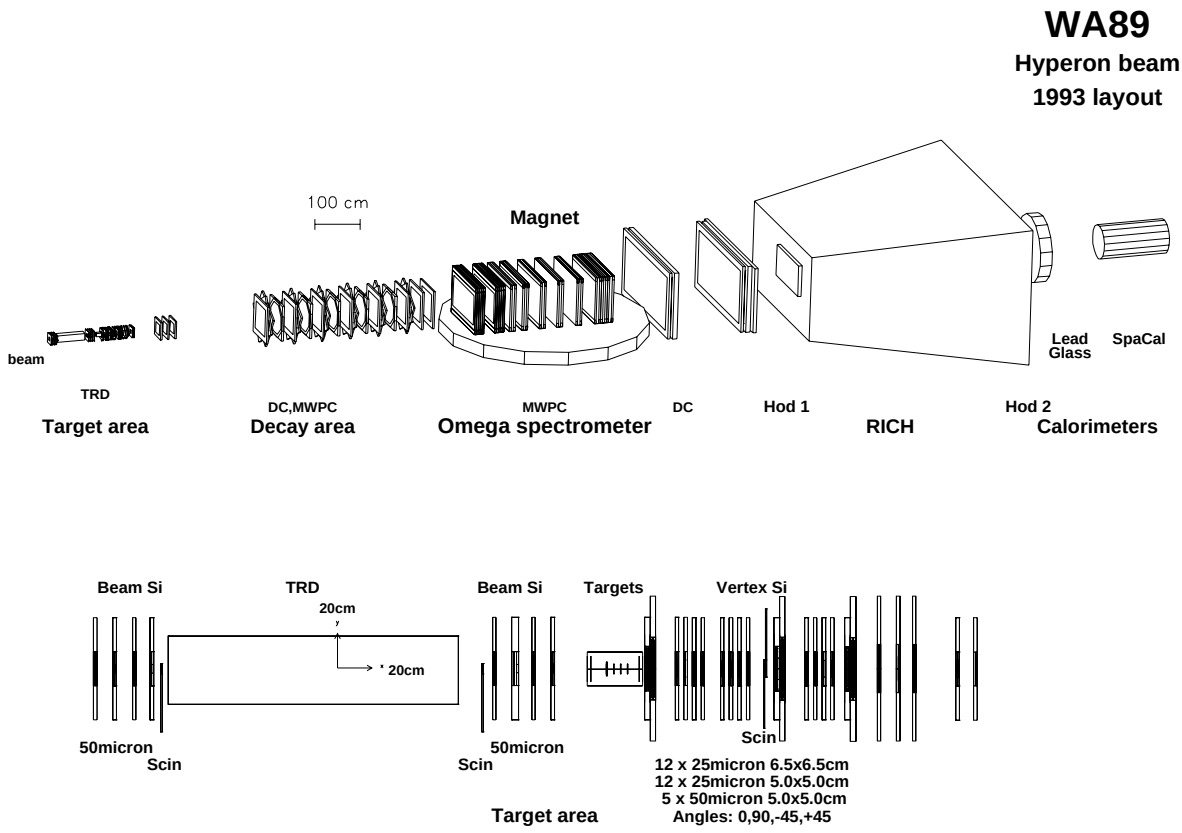

Fig. 1. Setup of the WA89 experiment in the 1993 run. The lower part shows an expanded view of the target area

a considerably stronger leading particle effect than observed in hyperon production by hyperons [3,4]. A different ansatz is used in the quark-gluon-string model (QGSM) [5,6], and we will compare our data with predictions from both models.

In previous publications [3,4], we have already presented data on Ξ and Ξ^* production by Σ^-, neutrons and π^-. We now present measurements of $\Sigma^{\pm}$, $\Sigma^{*\pm}$ and $\overline{\Sigma}^{-}_{1385}$ production by the same beams.

Thus, there exists now a large set of experimental data on the inclusive production of Σ, Σ^*, $\overline{\Sigma}^*$, Ξ and Ξ^* by different beams, coming from one experiment. Together with the existing data on inclusive hyperon production by protons ([7]–[16]), π^- ([17]– [19]), K^- ([20]–[24]) and by Ξ^- ([1], [25]–[27]), they will allow detailed tests of the different models proposed and thereby help to improve our understanding of these complex processes.

2 Hyperon beam and experimental apparatus

The hyperon beam was derived from an external proton beam of the CERN-SPS, hitting a hyperon production target placed 16m upstream of the experimental target. Negative secondaries with a mean momentum of 345 GeV/c and a momentum spread $\sigma(p)/p \approx 9\%$ were selected in a magnetic channel. The production angles relative to the proton beam were smaller than 0.5 mrad. At the experimental target, the beam consisted of π^-, K^-, Σ^- and Ξ^- in the ratio 2.3: 0.025: 1: 0.012. A transition radiation detector (TRD) made up of 10 MWPCs interleaved with foam radiators allowed to select Σ^- or π^- at the trigger level. Typically, about $1.8 \cdot 10^5$ Σ^- and $4.5 \cdot 10^5$ π^- were delivered to the target during one SPS-spill, which had an effective length of about 1.5 s.

Σ^- decays upstream of the target were a source of neutrons used in our measurement as a neutron beam. The momenta of these neutrons were defined as the difference between the average Σ^- momentum and the momentum of the associated π^- measured in the spectrometer. The neutron spectrum had an average momentum of 260 GeV/c and a width of $\sigma(p)/p = 15\%$. More details can be found in [28]. An overview of the apparatus is shown in Fig. 1. The experimental target was situated 3.6m downstream of the exit of the last beam magnet. It consisted of one copper and three carbon blocks arranged in a row along the beam, with thicknesses corresponding to 0.026 λ_I and three times 0.0083 λ_I, resp. At the target, the Σ^-/π^- beam had a width of 3 cm and a height of 1.7 cm. The neutron beam was slightly wider since the maximum neutron decay angle in the decays of Σ^- of momentum 340 GeV/c is 0.7 mrad only, and the neutrons originated from Σ^- decaying on the last 5m upstream of the target. Microstrip detectors upstream and downstream of the target allowed to measure the tracks of the incoming beam particles and of the charged particles produced in the target blocks. The target was positioned 14m upstream of the centre of the Omega spectrometer magnet [29] so that

a field-free decay region of 10m length was provided for hyperon and K_S decays. Tracks of charged particles were measured inside the magnet and in the field-free regions upstream and downstream by MWPCs and driftchambers, with a total of 130 planes. The Omega magnet provided a field integral of 7.5 Tm, and the momentum resolution achieved was $\sigma(p)/p^2 \approx 10^{-4}$ (GeV/c)$^{-1}$.

Downstream of the spectrometer, a ring-imaging Cherenkov detector, an electromagnetic calorimeter and a hadron calorimeter (SPACAL) [30] were placed.

The hadron calorimeter consisted of a lead structure with interleaved layers of 2.2 m long plastic scintillating fibres placed in beam direction (so-called "spaghetti" geometry). Each group of 1141 fibres formed a hexagonal tower and had a common photomultiplier. There were 155 towers in total. The energy resolution was $\sigma_E/E = ((63 \pm 9)/\sqrt{E} + 18)\%$ and the spatial accuracy was $\sigma_{sp} = ((6.0 \pm 0.9)/\sqrt{E} + 0.5)cm$, where E is the neutron energy in units of GeV. A scintillating tile hodoscope was placed 15 cm upstream of the SPACAL calorimeter. The hodoscope was made out of 127 hexagonal tiles with the same granularity as the tower structure of the calorimeter. This hodoscope was used to suppress showers produced by charged hadrons. Details about the neutron shower reconstruction can be found in [31]. The hadron calorimeter was used for the identification of neutrons coming from $\Sigma^{\pm} \to n\pi^{\pm}$ decays and their energy measurements.

The main trigger selected about 25% of all interactions, using multiplicities measured in microstrip counters upstream and downstream of the target and in scintillator hodoscopes and MWPCs behind the Omega magnet. Correlations between hits in different detectors were used in the trigger to increase the fraction of events with high-momentum particles, thus reducing background from low-momentum pions in the beam. Beam Σ^- were identified online by the TRD. A sample of pion interactions was obtained by inverting the online TRD decision for a fraction of the runs. In addition, a reduced sample of beam triggers was recorded for trigger calibration purposes. The results presented in this article are based on 93 million Σ^- interactions, 7 million neutron interactions and 6 million π^- interactions recorded in 1993.

3 Event selection

Different reconstruction procedures had to be used for the $\Sigma^{\pm}$ ground states and for the excited states. The $\Sigma^{\pm}$ ground states were reconstructed from $\Sigma \to n\pi$ decays. The $\Sigma^{\pm}$ and $\pi^{\pm}$ tracks were reconstructed in the field-free region upstream of the spectrometer magnet, and the $\pi^{\pm}$ momentum was measured in the spectrometer. The neutron energy and its impact point were measured in the SPACAL calorimeter downstream of the spectrometer.

The $\Sigma^{*\pm}$ resonances, on the other hand, were reconstructed exclusively from their charged daughter particles in the decay chain $\Sigma^{*\pm} \to \Lambda\pi^{\pm}$, $\Lambda \to p\pi^-$. The Λ had to decay upstream of the spectrometer magnet and all daughter particle momenta were measured in the spectrometer.

3.1 Beam and vertex reconstruction

The interaction vertex was reconstructed from at least two charged particle tracks emerging from the targets (so-called "outgoing tracks"). Outgoing tracks were accepted even if they were reconstructed only in the microstrip counters downstream of the target and were not connected with a track segment in the decay region chambers. The reconstructed vertex position had to be within a target block where in each coordinate an additional margin of 3σ was allowed.

For Σ^- and π^- beam interactions, the transverse distance between the beam track and the reconstructed vertex position was required to be less than 6σ ($\sigma \approx 25\mu m$).

In the case of neutron interactions the beam track was assumed to come from a Σ^- decay upstream of the target, and it therefore had to miss the reconstructed interaction point by a distance of at least 6σ. This π^- candidate track had to be connected to a negative particle track in the spectrometer with a momentum smaller than 140 GeV/c corresponding to the $\Sigma^- \to n\pi^-$ decay kinematics at $< p > \approx 345$ GeV/c.

3.2 $\Sigma^{\pm}$ candidate reconstruction

The search for $\Sigma^{\pm} \to n\pi^{\pm}$ decay candidates started with hadron shower reconstruction in the SPACAL calorimeter. A special pattern recognition algorithm combined hits in several SPACAL elements into a shower and calculated the impact point and the shower energy. A hadronic shower was accepted as coming from a neutron if: a) none of the charged particle tracks reconstructed downstream of the spectrometer matched the barycenter of the shower within $3\sigma_{sp}$ of the calorimeter spatial resolution; b) the deposited energy was above 20 GeV. For more details see [31].

Next, a $\Sigma^{\pm}$ decay vertex (kink) was searched for, defined as an intersection of two tracks in the field-free region between the target and the spectrometer. The $\Sigma^{\pm}$ candidate track had to come from the interaction vertex and was not allowed to be linked to a track in the spectrometer. The $\pi^{\pm}$ candidate track had to be reconstructed in the spectrometer and was not allowed to be linked to a track in the target region.

The distance between these two tracks at the decay point had to be smaller than $3 \cdot \sigma \approx 0.3$ cm inferred from the simulation. The kink position and the shower barycenter and energy were used to calculate the neutron momentum. The resulting effective $n\pi^{\pm}$ mass plots are shown in Fig. 2. The estimated selection efficiency of $\Sigma^{\pm}$ is about 1%. The signals will be discussed below.

3.3 Σ^* candidate reconstruction

A clean sample of Λ decays was selected from V^0s visible upstream of the magnet. The closest distance between the reconstructed Λ track and the interaction vertex had to be less than 1.2 cm. The reconstructed $p\pi^-$ mass had

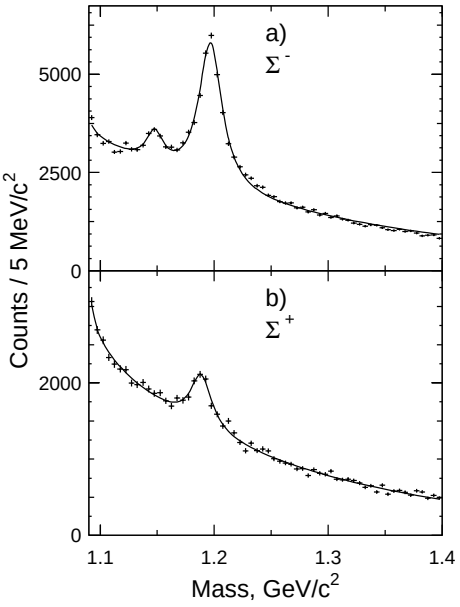

Fig. 2a,b. The $n\pi^{\pm}$ effective mass distributions

to be within $\pm 15\,\mathrm{MeV/c^2}$ of the Λ mass, where the error on the effective mass typically was $\sigma_m = 2.2\,\mathrm{MeV/c^2}$. These cuts were optimized on the observed Σ^* signals. Analogous cuts were used to obtain a sample of $\overline{\Lambda}$ decays. Finally, Λ candidates with a momentum of more than 260 GeV/c were rejected to suppress Λ from Ξ^- decays in the beam.

Σ^* candidates were obtained from all combinations of accepted Λ candidates with charged tracks coming from the primary vertex, assuming them to be pions.

4 $\Sigma^{\pm}$ and Σ^* signal determination

Figure 2 shows the $n\pi^{\pm}$ effective mass distributions. Clear signals from both Σ^- and Σ^+ are seen at the corresponding masses above a smooth background. The smaller signal at 1148 $\mathrm{MeV/c^2}$ in the $\Lambda\pi^-$ effective mass distribution comes from $\Xi^-\to\Lambda\pi^-$ decays, where the Λ particle survived into the hadron calorimeter and was taken as a neutron. The mass distributions were fitted by Gaussian functions for the signals and a simple exponential for the background. The mass resolutions are dominated by the SPACAL energy and position resolution, they and the central masses were left as free parameters in the fit. The masses from the fit are in good agreement with the known Σ^- and Σ^+ masses (see Table 2).

The effective mass distributions for $\Lambda^0\pi^{\pm}$ combinations are shown in Fig. 3. The distributions were fitted with Voigt functions for the two resonances (a convolution of a Breit-Wigner for the intrinsic width of the resonance and a gaussian for the mass resolution of the apparatus). The shape of the background was determined by "event mixing", where Λ^0 candidates were combined with charged tracks from different events also containing a Λ^0. The normalization of the background was left as

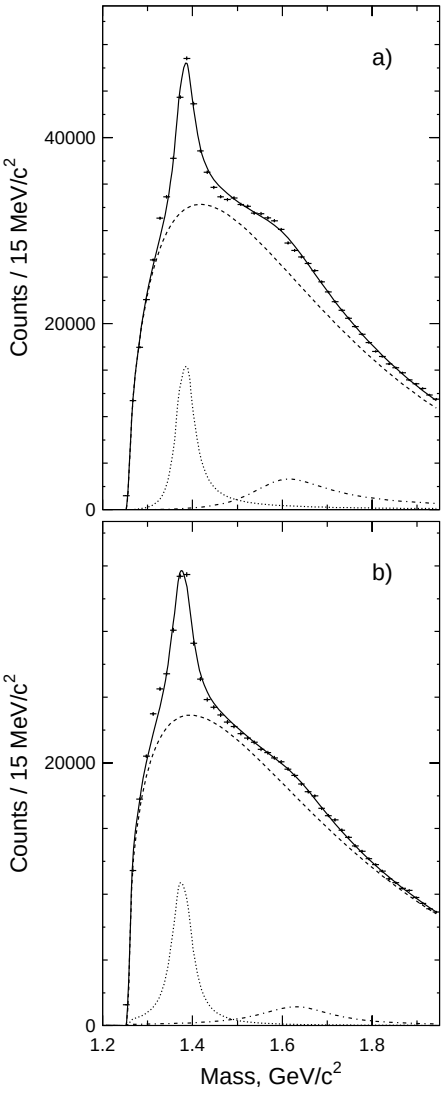

Fig. 3a,b. $\Lambda\pi^-$ **a** and $\Lambda\pi^+$ **b** effective mass distributions for $x_F > 0.3$. Separately shown are the contributions from resonances (dotted and dash-dotted curves) and the background (dashed curve) as estimated from event mixing. The solid curves represent the overall fit

a fit parameter. The fit results are shown in Fig. 3 and summarized in Table 1. In the fit of the resonances, we either set the mass resolutions to their Monte Carlo values and left the resonance widths as a free parameters, or we used the table values for the widths of the $\Sigma^{\pm}_{1385}$ [36] and a fixed value of 200 $\mathrm{MeV/c^2}$ for the widths of the $\Sigma^{\pm}_{1660}$ and left the mass resolutions as a free parameters. We also counted the number of events above background within the resonanse width region without using the result of the fit. The numbers of signal events determined by these three methods agreed within the respective errors.

The narrow peaks around 1385 $\mathrm{MeV/c^2}$ clearly correspond to the well-known decuplet Σ^*. The intrinsic widths of peaks corresponds to 35.8 ± 0.8 $\mathrm{MeV/c^2}$ for the Σ^+_{1385} and 39.4 ± 2.1 $\mathrm{MeV/c^2}$ for the Σ^-_{1385} with the mass resolution of the apparatus - $\sigma \approx (5. \pm 1.) MeV/c^2$. In MC

Table 1. Numbers of reconstructed events and total inclusive production cross sections per nucleus (σ_{nucl}) and nucleon (σ_0). α is the exponent describing the cross section dependence on the target mass number. Cross sections are for $0 \leq x_F \leq 1$, unless noted otherwise

particle	target	statistic	σ_{nucl} [mb]	σ_0 [mb]	α
			Σ^- beam		
Σ^-	Cu	30236 ± 291	123.83 ± 3.22		
	C	28109 ± 292	46.16 ± 1.12		
	nucleon			10.6 ± 0.8	0.59 ± 0.02
Σ^+	Cu	4605 ± 197	39.78 ± 1.95		
	C	4278 ± 206	12.25 ± 0.68		
	nucleon			2.1 ± 0.3	0.71 ± 0.04
Σ^-_{1385}	Cu	103566 ± 1093	27.01 ± 0.43		
	C	116275 ± 1063	10.20 ± 0.15		
	nucleon			2.4 ± 0.1	0.58 ± 0.01
Σ^+_{1385}	Cu	73770 ± 963	14.5 ± 0.4		
	C	80072 ± 1046	5.3 ± 0.1		
	nucleon			1.18 ± 0.06	0.60 ± 0.01
$\overline{\Sigma}^-_{1385}$	Cu	3874 ± 288	1.49 ± 0.12		
	C	3230 ± 240	0.42 ± 0.03		
	nucleon			0.06 ± 0.01	0.76 ± 0.06
Σ^-_{1660}	Cu	56278 ± 812	7.1 ± 0.2		
$\sigma \cdot BR(\Lambda\pi^-)$	C	60414 ± 827	2.8 ± 0.1		
$0.3 \leq x_F \leq 1$	nucleon			0.7 ± 0.1	0.56 ± 0.02
Σ^+_{1660}	Cu	30510 ± 530	2.0 ± 0.1		
$\sigma \cdot BR(\Lambda\pi^+)$	C	33450 ± 543	0.8 ± 0.04		
$0.3 \leq x_F \leq 1$	nucleon			0.2 ± 0.02	0.53 ± 0.03
			π^- beam		
$\Sigma^-_{1385} \to \Lambda\pi^-$	Cu	2608 ± 196	5.28 ± 0.49		
	C	2631 ± 198	1.80 ± 0.14		
	nucleon			0.36 ± 0.08	0.65 ± 0.07
$\Sigma^+_{1385} \to \Lambda\pi^+$	Cu	2091 ± 177	3.91 ± 0.37		
	C	1739 ± 147	1.01 ± 0.12		
	nucleon			0.13 ± 0.04	0.81 ± 0.09
			neutron beam		
$\Sigma^-_{1385} \to \Lambda\pi^-$	Cu	3222 ± 177	25.10 ± 1.75		
	C	3063 ± 169	8.262 ± 0.52		
	nucleon			1.6 ± 0.3	0.67 ± 0.05
$\Sigma^+_{1385} \to \Lambda\pi^+$	Cu	2002 ± 162	9.23 ± 1.08		
	C	1803 ± 146	2.69 ± 0.28		
	nucleon			0.4 ± 0.1	0.74 ± 0.09

Table 2. Reconstructed masses, widths and apparatus mass resolutions

particle	mass MeV/c^2	Γ MeV/c^2	σ_{Data} MeV/c^2	σ_{MC} MeV/c^2
$\Sigma^- \to n\pi^-$	1196.6 ± 0.2	–	5.6 ± 0.1	–
$\Sigma^+ \to n\pi^+$	1188.2 ± 0.6	–	5.5 ± 0.4	–
$\Sigma^-_{1385} \to \Lambda\pi^-$	1389.3 ± 0.1	–	5. ± 1.	6. ± 1.
$\Sigma^+_{1385} \to \Lambda\pi^-$	1385.2 ± 0.2	–	5. ± 1.	6. ± 1.
$\Sigma^-_{1660} \to \Lambda\pi^-$	1632. ± 8.	199. ± 45.	–	11. ± 1.
$\Sigma^+_{1660} \to \Lambda\pi^+$	1635. ± 10.	195. ± 54.	–	11. ± 1.

calculations the mass resolution was estimated to be $\sigma \approx 6$ MeV/c^2 for both states (Table 2).

A second, wider resonance appears above 1600 MeV/c^2 in both the $\Lambda\pi^+$ and the $\Lambda\pi^-$ channel. We will denote these resonances as Σ_{1660}. The observed signals are more significant at high $x_F > 0.6$, as shown in Fig. 4.

Owing to its much larger width its separation from the background is more difficult, with correspondingly large errors on mass and width. These signals were fitted in the same way as the $\Sigma^{\pm}_{1385}$ peaks, with the results listed in Table 2. The statistical errors are rather small for both Σ_{1660} resonances, but the uncertainties on the background

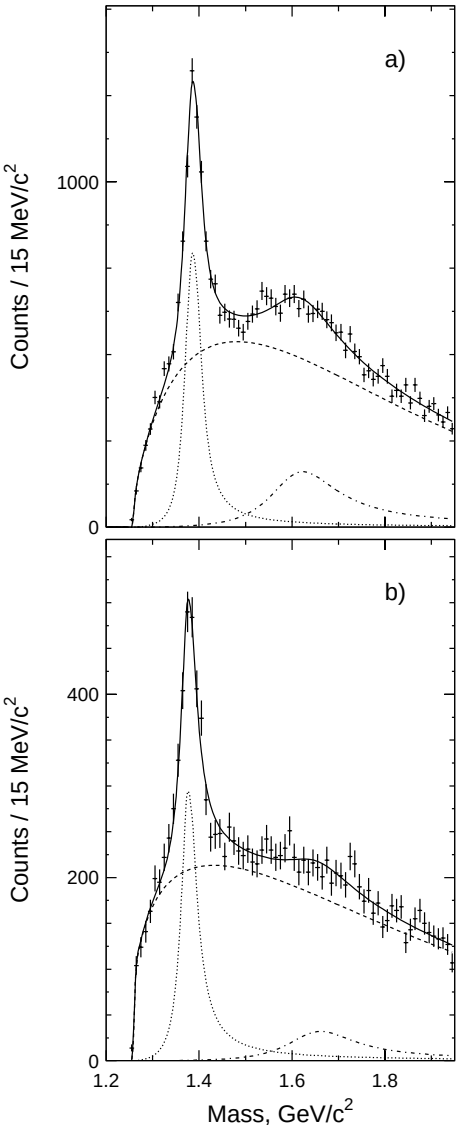

Fig. 4a,b. $\Lambda\pi^-$ **a** and $\Lambda\pi^+$ **b** effective mass distributions at high $x_F > 0.6$

subtraction provide large systematic contributions. This reduces the statistical significance of the Σ^-_{1660} and the Σ^+_{1660} signals to 7.4 and 4.8 standard deviations, resp.At high $x_F > 0.6$ these resonances become more significant 15 and 6.5 standart deviations resp. The physical interpretation of these signals will be discussed below.

Finally, we show in Fig. 5 the $\overline{\Lambda}\pi^-$ mass spectrum, which exhibits a clear $\overline{\Sigma}^-_{1385}$ signal at around 1385 MeV/c^2.

5 The Σ production cross sections

The production cross sections of $\Sigma^{\pm}_{1385}$ were determined for the Σ^-, π^- and neutron beam, while for the other states only the Σ^- beam data had sufficient statistics for a cross section measurement. In the following, we will discuss the corrections for the beam contaminations [28].

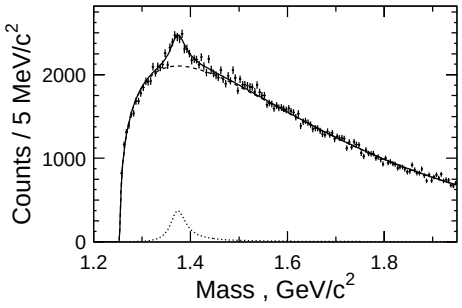

Fig. 5. $\overline{\Lambda}^0\pi^-$ effective mass distribution

The Σ^- beam, tagged by the TRD, had a contamination of (12±2)% of fast π^-, (2.0±0.5)% of K^- and (1.3±0.3)% of Ξ^-. The distortions of the cross section measurements expected from the K^- and Ξ^- contents are insignificant and will be neglected here. In $\Sigma^{\pm}_{1385}$ production, the effect of the pion contamination was corrected for using our measurements of $\Sigma^{\pm}_{1385}$ production in the pion beam. The production cross sections for the other particles, which were measured for the Σ^- beam only, were corrected by assuming the ratio of production by Σ^- and π^- to be the same as measured for $\Sigma^{\pm}_{1385}$ production.

The π^- beam, tagged by the TRD, contained about 1% of Σ^- and negligible fractions of K^- and Ξ^-. The small effects from the Σ^- contamination were corrected for using the measured Σ^- beam data.

The neutron beam contained an admixture of Λ from Ξ^- decays in the beamline. Since the decay lengths of Σ^- and Ξ^- of equal momenta happen to agree within 1%, the Λ/n ratio is equal to the Ξ^-/Σ^- ratio in the beam, which was measured to be 1.2%. This small contamination can safely be neglected here.

For the absolute normalization of the cross sections, systematic errors from the uncertainties of the efficiency determination (15%) and the trigger simulation (10%) have to be added. For a given particle produced, these uncertainties are highly correlated between different bins of $x_F$and $p_t$resp., as determined from MC simulations. We therefore prefer to plot and fit the $x_F$and $p_t$distributions shown in Fig. 6–10 (for carbon target only) and listed in Tables 4–13 without these systematic errors and to add a total systematic error of 20% to the integrated cross sections listed in Table 1.

The differential cross sections as a function of the x_F or p_t^2 were parametrised by functions of the form:

$$\frac{d\sigma}{dx_F} \propto (1 - x_F)^n \tag{1}$$

or

$$\frac{d\sigma}{dp_t^2} \propto exp(-Bp_t^2), \tag{2}$$

which is based on quark counting rules and phase space arguments [38]. The parameters n and B were assumed to be independent of p_t^2 and x_F. The values of n and B obtained from the fits are listed in Table 3 for each target, and the fits are shown in Fig. 6–10 as straight lines over the

Table 3. Parameter values of the differential cross sections fitted as $d\sigma/dx_F \propto (1-x_F)^n$ or $d\sigma dp_t^2 \propto exp(-Bp_t^2)$, resp

particle	Beam target	Σ^- n	Σ^- B	π^- n	π^- B	Neutrons n	Neutrons B
$\Sigma^-\to n\pi^-$	Cu	-0.87 ± 0.09	2.47 ± 0.08	–	–	–	–
	C	-1.23 ± 0.09	2.34 ± 0.08	–	–	–	–
$\Sigma^+\to n\pi^+$	Cu	1.7 ± 0.2	2.5 ± 0.2	–	–	–	–
	C	1.6 ± 0.2	2.5 ± 0.2	–	–	–	–
$\overline{\Sigma}^-_{1385}\to\Lambda\pi^-$	Cu	0.61 ± 0.04	1.97 ± 0.04	1.9 ± 0.4	1.9 ± 0.3	0.4 ± 0.1	1.9 ± 0.2
	C	0.42 ± 0.03	2.05 ± 0.03	1.4 ± 0.2	2.0 ± 0.3	0.4 ± 0.1	2.1 ± 0.3
$\Sigma^+_{1385}\to\Lambda\pi^+$	Cu	1.12 ± 0.04	1.84 ± 0.04	1.8 ± 0.3	2.3 ± 0.4	1.8 ± 0.2	1.6 ± 0.2
	C	0.88 ± 0.04	2.13 ± 0.04	1.8 ± 0.3	2.4 ± 0.5	2.2 ± 0.2	1.9 ± 0.2
$\overline{\Sigma}^-_{1385}\to\overline{\Lambda}\,\pi^-$	Cu	4.4 ± 0.4	2.3 ± 0.2	–	–	–	–
	C	3.9 ± 0.4	1.9 ± 0.2	–	–	–	–
$\Sigma^-_{1660}\to\Lambda\pi^-$	Cu	0.6 ± 0.1	1.3 ± 0.2	–	–	–	–
	C	0.5 ± 0.1	1.4 ± 0.2	–	–	–	–
$\Sigma^+_{1660}\to\Lambda\pi^+$	Cu	4.1 ± 0.8	2.1 ± 0.3	–	–	–	–
	C	3.9 ± 0.7	2.2 ± 0.3	–	–	–	–

Table 4. Differential production cross sections of Σ^- and Σ^+ by Σ^- as a function of x_F in mb

x_F	Σ^- copper	Σ^- carbon	Σ^+ copper	Σ^+ carbon
0.1 - 0.2	$117. \pm 9.$	$37. \pm 3.$	$112. \pm 28.$	$29. \pm 9.$
0.2 - 0.3	$125. \pm 6.$	$46. \pm 2.$	$95. \pm 14.$	$28. \pm 5.$
0.3 - 0.4	$170. \pm 7.$	$56. \pm 2.$	$72. \pm 10.$	$25. \pm 3.$
0.4 - 0.5	$176. \pm 8.$	$76. \pm 3.$	$56. \pm 8.$	$18. \pm 3.$
0.5 - 0.6	$195. \pm 10.$	$80. \pm 4.$	$36. \pm 7.$	$14. \pm 2.$
0.6 - 0.7	$199. \pm 15.$	$87. \pm 6.$	$26. \pm 8.$	$7. \pm 3.$
0.7 - 0.8	$257. \pm 30.$	$79. \pm 9.$	–	–

Table 5. Differential production cross sections of Σ^- and Σ^+ by Σ^- as a function of p_t^2 in mb/(GeV/c)^2

p_t^2	Σ^- copper	Σ^- carbon	Σ^+ copper	Σ^+ carbon
0.0 - 0.2	$247. \pm 8.$	$94. \pm 3.$	$80. \pm 8.$	$26. \pm 3.$
0.2 - 0.4	$127. \pm 5.$	$50. \pm 2.$	$46. \pm 6.$	$11. \pm 2.$
0.4 - 0.6	$85. \pm 5.$	$32. \pm 2.$	$28. \pm 5.$	$8. \pm 1.$
0.6 - 0.8	$58. \pm 5.$	$22. \pm 2.$	$16. \pm 4.$	$6. \pm 1.$
0.8 - 1.0	$35. \pm 4.$	$11. \pm 1.$	$13. \pm 4.$	$3. \pm 1.$
1.0 - 1.2	$27. \pm 4.$	$7. \pm 1.$	$5. \pm 3.$	$3. \pm 1.$
1.2 - 1.4	$15. \pm 3.$	$7. \pm 1.$	$8. \pm 3.$	$2. \pm 1.$
1.4 - 1.6	$18. \pm 4.$	$4. \pm 1.$	$4. \pm 1.$	$2. \pm 0.8$
1.6 - 1.8	$10. \pm 4.$	$5. \pm 2.$	–	–

fit range. No significant difference is observed between the values obtained from the copper and the carbon target.

Figure 11a–e shows the nuclear mass dependence of Σ production as a function of x_F and p_t^2. The left-hand scales give the cross section ratio:

$$R = \frac{\sigma_{Cu}}{\sigma_C} \cdot \frac{A_C}{A_{Cu}} \tag{3}$$

The right-hand scales show the corresponding values of α in the usual parametrisation for the A dependence:

$$\sigma = \sigma_0 \cdot A^{\alpha} \tag{4}$$

The dashed lines correspond to α=2/3 and α=1, respectively.

The values of α measured for the different combinations of beams and produced particles are very similar to each other and to those observed in other hadroproduction processes. The latter can be summarised as $\alpha(x_F) = 0.8 - 0.75x_F + 0.45x_F^2$ [39] (solid line in the left-side panels of Fig. 11a–e. Our data show no visible dependence of α on p_t^2 with the possible exception of $\overline{\Sigma}^-_{1385}$ production (Fig. 11e, right)

The total production cross sections per nucleus for $x_F > 0$ are listed in Table 1 for copper and carbon. The total production cross sections per nucleon for $x_F > 0$ were obtained by extrapolating the differential cross sections measured on Cu and C in each bin of x_F using the values of α obtained in the same bin. They are also listed in Table 1.

6 Discussion

In our experiment we observed the production of six Σ and one $\overline{\Sigma}$ states under the same conditions, which gives us a unique possibility to compare their production spectra.

While the $\Sigma^{\pm}, \Sigma^{\pm}_{1385}$ signals and even the $\overline{\Sigma}^-_{1385}$ signal are unambiguous, the interpretation of the wide peak observed around 1.63 GeV/c^2 is difficult.

Several candidates for excited Σ states were observed in the region of 1.6-1.8 GeV/c^2 as a result of differential

Table 6. Differential production cross sections of Σ^{-}_{1385} in different beams as a function of x_F in mb

Beam	Neutrons		π^-		Σ^-	
x_F	Copper	Carbon	Copper	Carbon	Copper	Carbon
0.0 - 0.1	45.2 ± 14.6	12.0 ± 4.0	9.3 ± 4.0	2.9 ± 1.1	20.8 ± 3.5	5.3 ± 0.9
0.1 - 0.2	30.3 ± 4.9	9.7 ± 1.7	11.0 ± 2.0	2.9 ± 0.7	28.4 ± 1.7	8.7 ± 0.5
0.2 - 0.3	28.0 ± 4.2	10.1 ± 1.5	5.6 ± 1.3	1.9 ± 0.3	41.7 ± 1.9	13.8 ± 0.6
0.3 - 0.4	25.1 ± 3.5	9.3 ± 1.3	2.8 ± 0.8	1.6 ± 0.3	38.2 ± 1.6	14.0 ± 0.5
0.4 - 0.5	17.8 ± 2.9	9.0 ± 1.4	1.4 ± 0.6	0.8 ± 0.2	37.0 ± 1.4	13.9 ± 0.5
0.5 - 0.6	20.9 ± 4.1	5.0 ± 1.2	1.1 ± 0.7	0.3 ± 0.2	29.9 ± 1.2	12.9 ± 0.5
0.6 - 0.7	–	–	–	–	23.4 ± 0.9	10.7 ± 0.4
0.7 - 0.8	–	–	–	–	19.2 ± 0.9	9.3 ± 0.4
0.8 - 0.9	–	–	–	–	20.1 ± 1.4	7.9 ± 0.5
0.9 - 1.0	–	–	–	–	11.3 ± 1.9	5.6 ± 0.8

Table 7. Differential production cross section of Σ^{-}_{1385} in different beams as a function of p_t^2 in mb/(GeV/c)^2

Beam	Neutrons		π^-		Σ^-	
p_t^2	Copper	Carbon	Copper	Carbon	Copper	Carbon
0.0 - 0.3	35.8 ± 4.3	14.1 ± 1.7	9.5 ± 2.1	2.5 ± 0.6	41.7 ± 0.9	15.7 ± 0.3
0.3 - 0.6	20.8 ± 2.9	5.6 ± 1.2	4.9 ± 1.6	2.2 ± 0.5	21.1 ± 0.6	8.1 ± 0.2
0.6 - 0.9	7.9 ± 1.8	2.8 ± 0.8	4.0 ± 1.1	1.9 ± 0.4	10.9 ± 0.4	4.4 ± 0.2
0.9 - 1.2	5.5 ± 1.7	2.2 ± 0.6	3.6 ± 0.9	0.6 ± 0.2	7.3 ± 0.3	2.5 ± 0.1
1.2 - 1.5	6.4 ± 1.5	1.6 ± 0.6	1.7 ± 0.8	0.6 ± 0.2	3.8 ± 0.2	1.4 ± 0.1
1.5 - 1.8	3.5 ± 1.2	0.7 ± 0.4	0.8 ± 0.6	0.4 ± 0.2	2.8 ± 0.2	0.7 ± 0.1
1.8 - 2.1	2.0 ± 0.9	0.4 ± 0.3	–	–	1.5 ± 0.1	0.5 ± 0.1
2.1 - 2.4	–	–	–	–	1.2 ± 0.1	0.2 ± 0.1

Table 8. Differential production cross section of Σ^{+}_{1385} in different beams as a function of x_F in mb

Beam	Neutrons		π^-		Σ^-	
x_F	Copper	Carbon	Copper	Carbon	Copper	Carbon
0.0 - 0.1	20.3 ± 9.4	5.6 ± 2.2	12.8 ± 3.2	2.3 ± 1.0	13.7 ± 2.3	5.5 ± 0.8
0.1 - 0.2	18.4 ± 4.3	6.3 ± 1.2	6.3 ± 1.4	1.7 ± 0.4	21.5 ± 1.4	6.6 ± 0.4
0.2 - 0.3	11.3 ± 2.5	3.3 ± 0.8	3.2 ± 0.9	1.3 ± 0.3	20.4 ± 1.2	7.5 ± 0.4
0.3 - 0.4	6.8 ± 1.4	1.8 ± 0.5	2.1 ± 0.6	0.8 ± 0.2	24.1 ± 1.1	8.7 ± 0.4
0.4 - 0.5	3.3 ± 0.9	0.6 ± 0.3	0.9 ± 0.4	0.3 ± 0.1	21.4 ± 0.9	7.1 ± 0.3
0.5 - 0.6	1.4 ± 0.4	0.2 ± 0.2	0.9 ± 0.4	0.3 ± 0.1	15.8 ± 0.7	5.9 ± 0.2
0.6 - 0.7	–	–	–	–	10.6 ± 0.5	4.1 ± 0.2
0.7 - 0.8	–	–	–	–	7.8 ± 0.5	3.8 ± 0.2

partial wave analyses (DPWA) of data obtained in bubble chamber experiments ([32] - [35]) with low momentum beams of 0.5 - 8 GeV/c. The usual number of solutions found was about 6-7.

In [18] there is also weak evidence for two peaks above 1600 MeV/c^2 in a $\Lambda\pi$ effective mass distribution. These peaks were attributed by the authors to the Σ_{1620} and Σ_{1690}.

It is thus quite likely that our observed wide signal is due to contributions from different (wide and overlapping) resonances. Since we are unable to separately determine their quantum numbers, we will treat our signal as coming from a single Σ-like state. Its position and its measured width of about 200 MeV/c^2 are compatible with the well-established resonance $\Sigma^{\pm}_{1660}$ ($I(J^P) = 1(1/2^+)$) [36]. For the width of this resonance, measured values range from 40±10 to 150±20 MeV/c^2. For the equally well-established Σ_{1670} ($I(J^P) = 1(3/2^-)$) [36], widths between 50±5 and 79±6 are quoted, which make it a less likely candidate for our peak.

The branching ratio of the decay $\Sigma^{\pm}_{1660} \rightarrow \Lambda\pi^-$ is not known, while the corresponding Σ_{1670} branching ratio was measured to be 5-15%. We therefore only quote our measured value for the product σ·BR in Table 1).

Table 9. Differential production cross section of Σ^{+}_{1385} in different beams as a function of p_t^2 in mb/(GeV/c)^2

Beam	Neutrons		π^-		Σ^-	
p_t^2	Copper	Carbon	Copper	Carbon	Copper	Carbon
0.0 - 0.3	10.9 ± 2.4	3.8 ± 0.7	7.2 ± 1.8	2.2 ± 0.4	20.5 ± 0.7	8.3 ± 0.2
0.3 - 0.6	8.9 ± 1.9	2.5 ± 0.5	4.5 ± 1.4	1.1 ± 0.3	12.2 ± 0.5	4.4 ± 0.2
0.6 - 0.9	4.4 ± 1.4	1.0 ± 0.4	4.1 ± 1.0	0.5 ± 0.3	6.8 ± 0.4	2.4 ± 0.1
0.9 - 1.2	2.0 ± 0.9	0.9 ± 0.3	2.1 ± 0.9	0.7 ± 0.2	3.8 ± 0.3	1.1 ± 0.1
1.2 - 1.5	1.8 ± 0.7	0.2 ± 0.2	1.2 ± 0.7	0.2 ± 0.2	2.3 ± 0.2	0.70 ± 0.06
1.5 - 1.8	1.0 ± 0.6	0.2 ± 0.1	0.4 ± 0.6	0.3 ± 0.2	1.3 ± 0.2	0.38 ± 0.05
1.8 - 2.1	1.3 ± 0.5	0.2 ± 0.1	–	–	0.8 ± 0.1	0.25 ± 0.03
2.1 - 2.4	0.4 ± 0.5	0.2 ± 0.1	–	–	0.6 ± 0.1	0.12 ± 0.02

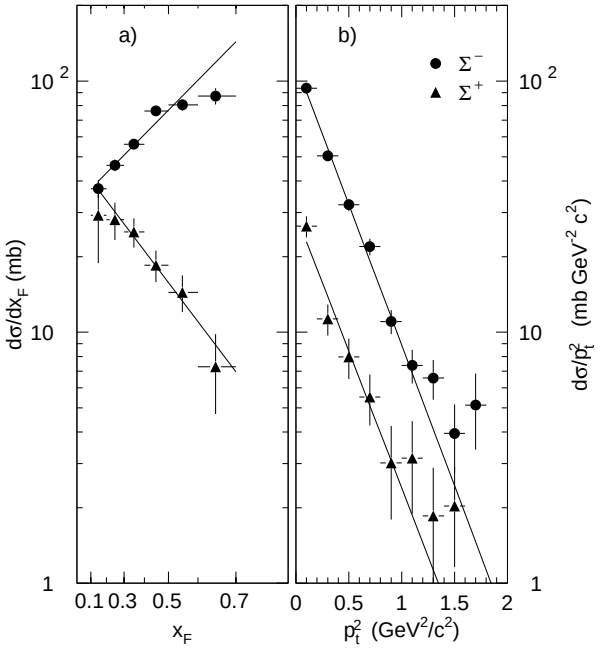

Fig. 6a,b. Differential cross sections of inclusive Σ^- and Σ^+ production by Σ^- in carbon

Table 10. Differential cross sections of $\overline{\Sigma}^{-}_{1385}$ production by Σ^- as a function of x_F in mb

x_F	copper	carbon
0.00 - 0.15	$5. \pm 1.$	1.5 ± 0.3
0.15 - 0.30	3.5 ± 0.5	0.8 ± 0.2
0.30 - 0.45	0.8 ± 0.3	0.3 ± 0.1
0.45 - 0.60	0.3 ± 0.2	0.06 ± 0.05
0.60 - 0.75	0.08 ± 0.09	0.08 ± 0.04

Nevertheless, we would like to point out that for the first time a statistically significant Σ^* in the region above 1.4 GeV/c^2 was observed in an effective mass distribution. In all previous publications, such resonances appeared only as solutions of sophisticated DPWA analyses.

In Fig. 12 we show on the left side the invariant cross sections of Σ production by Σ^- and for comparison, of proton production by protons [37] and Ξ^- production by

Table 11. Differential cross sections of $\overline{\Sigma}^{-}_{1385}$ production by Σ^- as a function of p_t^2 in mb/(GeV/c)^2

p_t^2	copper	carbon
0.0 - 0.3	2.5 ± 0.4	0.6 ± 0.1
0.3 - 0.6	1.2 ± 0.2	0.34 ± 0.07
0.6 - 0.9	0.7 ± 0.2	0.22 ± 0.06
0.9 - 1.2	0.2 ± 0.1	0.08 ± 0.04
1.2 - 1.5	0.10 ± 0.09	0.08 ± 0.03
1.5 - 1.8	0.22 ± 0.07	0.02 ± 0.02
1.8 - 2.1	0.05 ± 0.05	0.03 ± 0.01
2.1 - 2.4	0.04 ± 0.04	0.01 ± 0.01

Table 12. Differential production cross sections σ·BR of Σ^{-}_{1660} and Σ^{+}_{1660} by Σ^- as a function of x_F in mb

	Σ^{-}_{1660}		Σ^{+}_{1660}	
x_F	copper	carbon	copper	carbon
0.3 - 0.4	15.6 ± 1.9	5.9 ± 0.6	10.9 ± 1.4	4.3 ± 0.5
0.4 - 0.5	15.6 ± 1.6	4.9 ± 0.5	5.6 ± 1.1	2.0 ± 0.4
0.5 - 0.6	10.9 ± 1.4	4.8 ± 0.5	2.6 ± 0.8	1.0 ± 0.3
0.6 - 0.7	10.2 ± 1.1	4.3 ± 0.4	0.8 ± 0.7	0.3 ± 0.3
0.7 - 0.8	7.1 ± 1.0	3.3 ± 0.4	0.3 ± 0.7	0.7 ± 0.3
0.8 - 0.9	8.0 ± 1.5	2.9 ± 0.5	–	–
0.9 - 1.0	3.3 ± 2.2	1.6 ± 0.8	–	–

Table 13. Differential production cross sections σ·BR of Σ^{-}_{1660} and Σ^{+}_{1660} by Σ^- as a function of p_t^2 in mb/(GeV/c)^2

	Σ^{-}_{1660} $0.3 \leq 1.$		Σ^{+}_{1660} $0.3 \leq 0.8$	
p_t^2	copper	carbon	copper	carbon
0.0 - 0.3	9.8 ± 1.4	3.3 ± 0.4	3.4 ± 0.6	1.3 ± 0.2
0.3 - 0.6	4.2 ± 1.1	2.1 ± 0.3	1.3 ± 0.4	0.6 ± 0.2
0.6 - 0.9	3.1 ± 0.8	1.3 ± 0.3	0.9 ± 0.3	0.5 ± 0.1
0.9 - 1.2	2.2 ± 0.7	1.0 ± 0.2	0.6 ± 0.3	0.1 ± 0.1
1.2 - 1.5	1.6 ± 0.5	0.8 ± 0.2	0.05 ± 0.2	0.1 ± 0.1
1.5 - 1.8	1.6 ± 0.4	0.3 ± 0.1	0.2 ± 0.2	0.01 ± 0.06
1.8 - 2.1	0.5 ± 0.3	0.4 ± 0.08	0.2 ± 0.1	0.08 ± 0.4
2.1 - 2.4	0.6 ± 0.3	0.14 ± 0.07	0.04 ± 0.09	0.03 ± 0.04

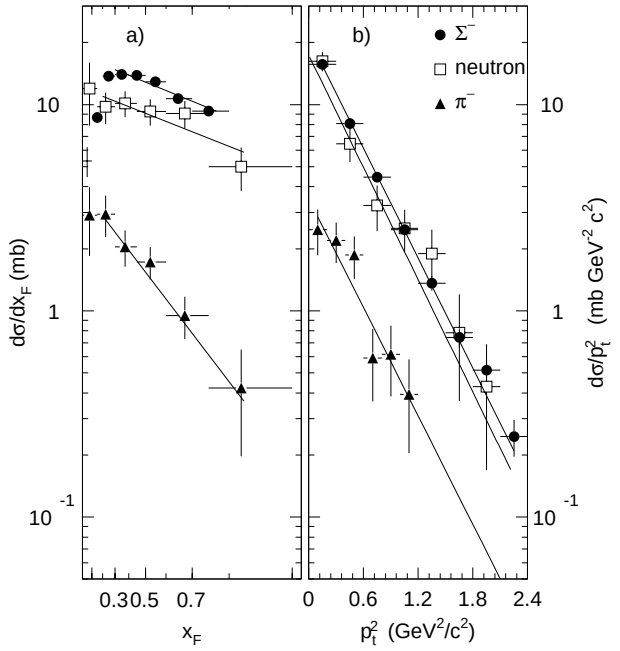

Fig. 7a,b. Differential cross sections of inclusive Σ^{-}_{1385} production by Σ^{-}, neutrons and π^{-} in carbon

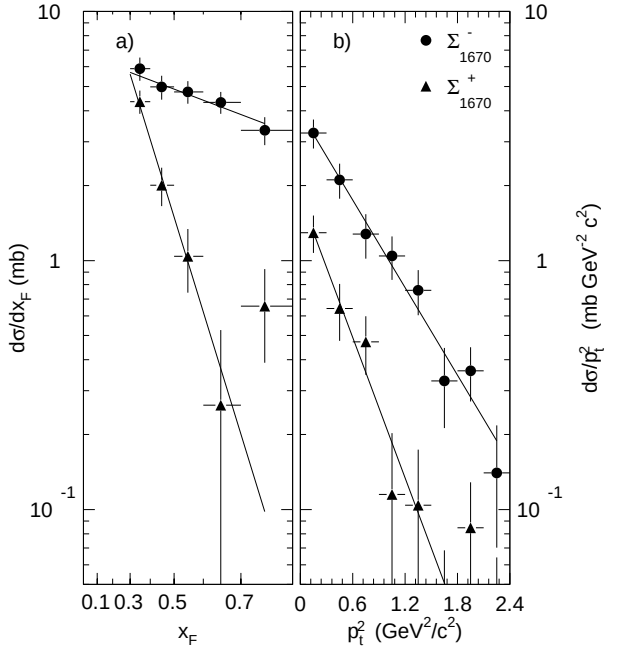

Fig. 9a,b. Differential cross sections of inclusive $\Sigma^{\pm}_{1660}$ production by Σ^{-} in carbon

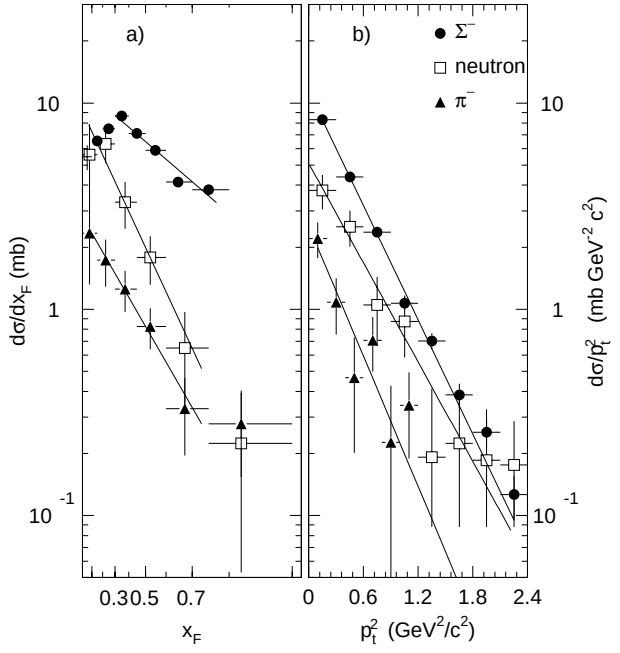

Fig. 8a,b. Differential cross sections of inclusive Σ^{+}_{1385} production by Σ^{-}, neutrons and π^{-} in carbon

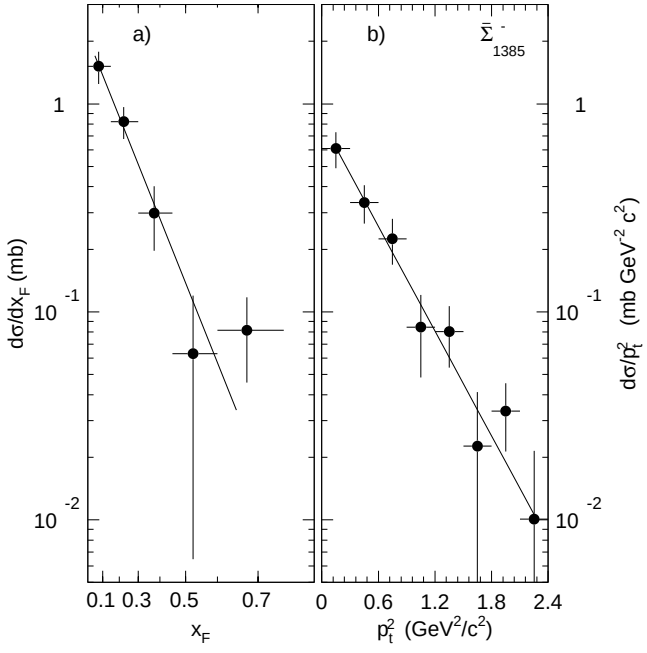

Fig. 10a,b. Differential cross sections of inclusive $\overline{\Sigma}^{-}_{1385}$ production by Σ^{-} in carbon

Ξ^{-} [1]. On the right side the invariant cross sections are shown for $\Sigma^{\pm}_{1385}$ production by π^{-} and neutrons.

At high x_F the production cross sections of the reactions with identical incoming and outgoing particle become very close. Compared to Σ^{-} production by Σ^{-}, Σ^{+} and $\Sigma^{\pm}_{1385}$ production is suppressed by about a factor 10. It is interesting to note that the difference between Σ^{+} and Σ^{+}_{1385} production seems to vanish at high x_F, while the difference between Σ^{-} and Σ^{-}_{1385} production even increases with x_F.

In Fig. 12b we see that at high x_F the cross sections for Σ^{-}_{1385} production by Σ^{-} and by neutrons are roughly equal. This result is quite surprising, since at high x_F the leading particle effect should prefer Σ^{-}_{1385} by Σ^{-} over production by neutrons. Both cross sections are larger by more than a factor of 10 than the cross sections for Σ^{+}_{1385}

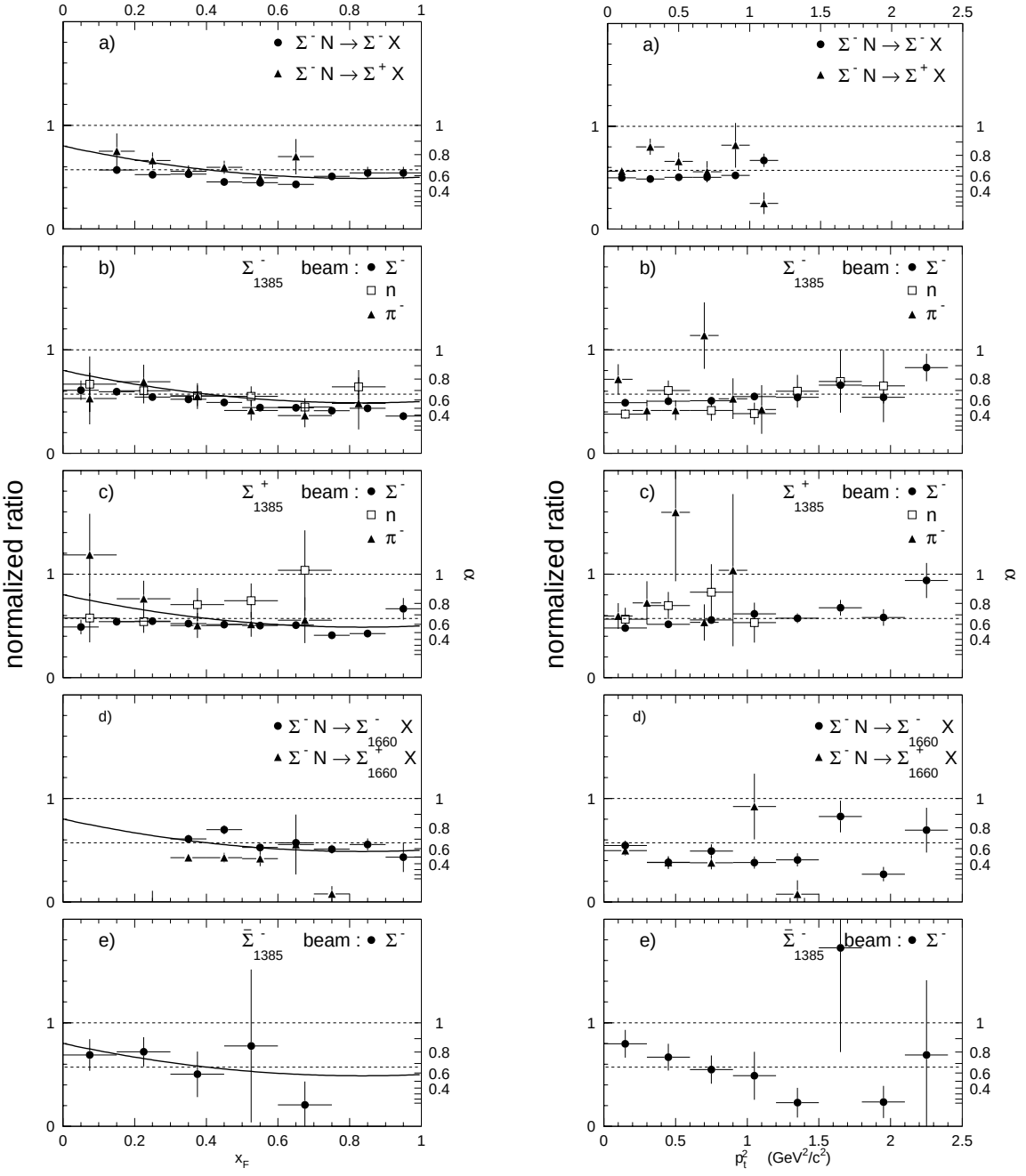

Fig. 11a–e. Normalized ratio R (see (3)) of $\Sigma^{\pm}$ production by Σ^- in copper and carbon as a function of x_F (left) and p_t^2 (right). The right scale indicates the exponent α in the A^{α} dependence. The solid line in the upper part shows a polynomial fit to a compilation of target attenuation factors given in [39]

production by neutrons and $\Sigma^{\pm}_{1385}$ production by π^-. The three latter cross sections are rather similar.

With the exception of Σ^-_{1385} production by Σ^- and neutrons, the leading particle effect, which predicts a strong dependence of the production cross sections on the valence quark overlap between beam particle and produced particle, is further confirmed by our data.

In a previous publication [4], we have reported on a systematical effect seen in the production of Ξ^- hyperon resonances: excited states seemed to show more leading behaviour, so that the slopes of the x_F spectra were monotonically decreasing with increasing degree of excitation. No such effect is observed in the present data with respect to the production of Σ^{*+} and Σ^{*-} hyperons, or is, at least, rather irregular (see Table 3). The data seem to be consistent with the assumption that the x_F spectra are universal, according to the identical quark content of all excited states.

At low x_F the cross section depends on the number of strange quarks in the product with a suppression factor

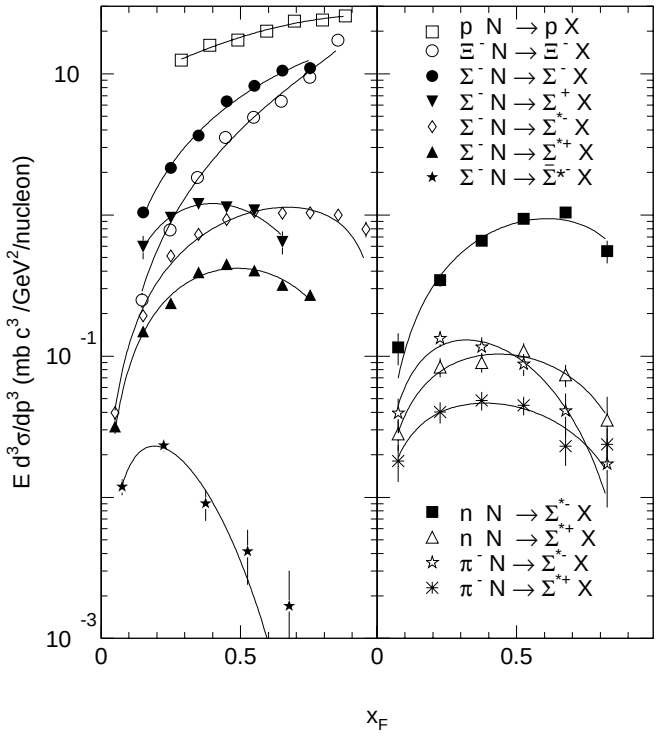

Fig. 12. Invariant cross sections for Σ, Σ^* and $\overline{\Sigma}^*$ production by $\Sigma^-\,\pi^-$ and neutrons. Also shown are $pA \to pX$ and $\Xi^- A \to \Xi^- X$ invariant production cross sections for comparison (see text)

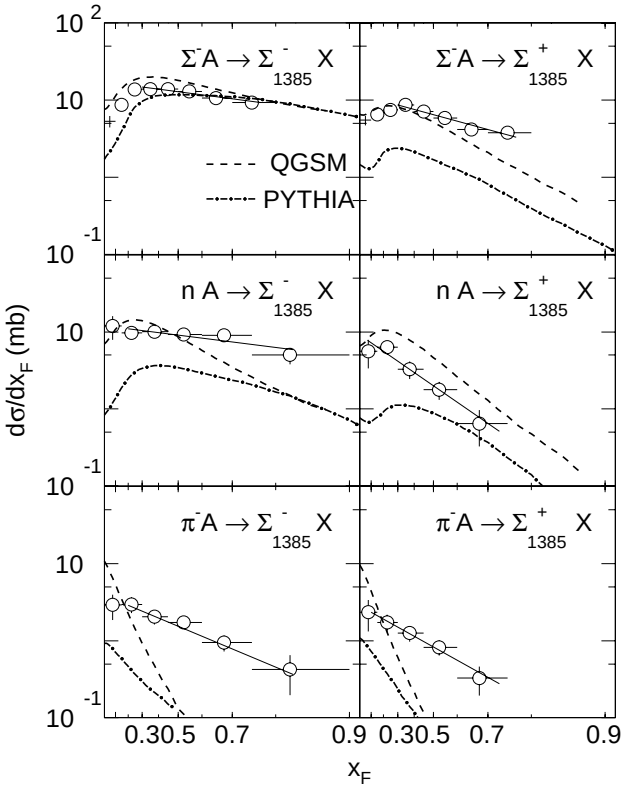

Fig. 13. Comparison of the measured differential cross section of $\Sigma^{\pm}_{1385}$ production in the carbon target with the predictions from PYTHIA and QGSM

of about 10 per strange quark. The production of $\Sigma^{\pm}_{1385}$ is suppressed w.r.t. the corresponding $\Sigma^{\pm}$ ground state by an additional factor of about 5. The differences between the $\Sigma^{\pm}_{1385}$ production cross sections by Σ^-, π^- and neutrons decrease steadily towards low x_F, regardless of the beam particle and the charge of the produced particle. This behaviour at low x_F, i.e. the strong dependence on the strangeness of the produced particle and the weak dependence on the nature of the beam particle, is also well-known from earlier hyperon production experiments.

The cross section for $\overline{\Sigma}^{-}_{1385}$ production by Σ^- at low x_F is smaller by perhaps a factor of 3 than the cross section for $\Sigma^{\pm}_{1385}$, but falls off very rapidly at higher x_F.

The p_t^2 spectra shown in Fig. 6b–10b have an exponential shape throughout the observed kinematical range $0 < p_t^2 < 1.5(\mathrm{GeV/c})^2$, with a slope parameter $B \approx (2.-2.3)$ $(\mathrm{GeV/c})^{-2}$for all Σstates produced and all beam particles.

In the following, we compare our measurements with calculations based on the Quark-Gluon String Model (QGSM) and on PYTHIA.

The Quark-Gluon String Model offers two free parameters (for each isotopic family) which are the probabilities to form the final state hadron via different fragmentation mechanisms. The baryon may be produced either directly from the projectile diquark, or indirectly in a remote part of the colour string (this includes quark, antiquark and antidiquark fragmentation cases, see [6] for more details). Although the absolute normalization of these two contributions is arbitrary, their x_F behaviour is strictly defined

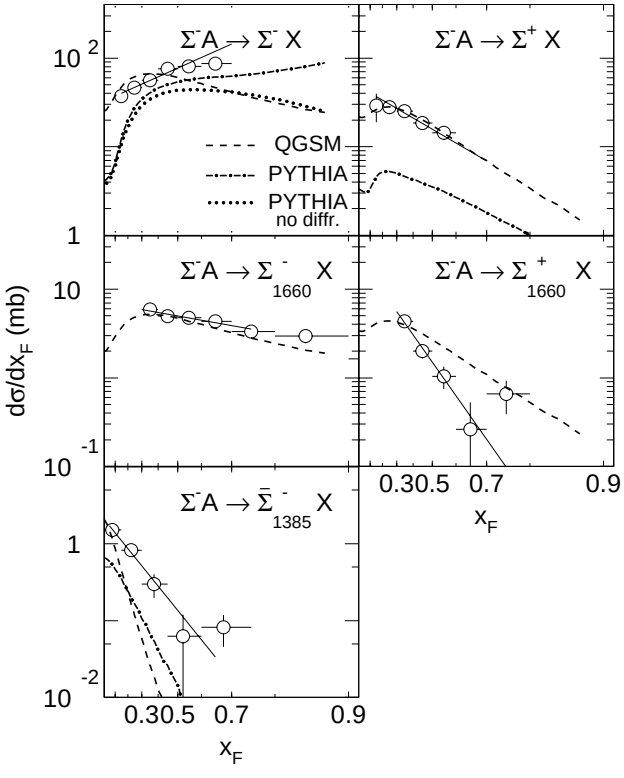

Fig. 14. Comparison of the measured differential cross section of $\Sigma^{\pm}$, $\Sigma^{\pm}_{1660}$ and $\overline{\Sigma}^{-}_{1385}$ production in the carbon target with the predictions from PYTHIA and QGSM

in the model. We have used the normalization freedom to tune the parameters to the measured differential cross section of the process $\Sigma^- C \rightarrow \Sigma^+ X$, which involves both direct and indirect fragmentation and is free from elastic contributions. Once fixed, these parameter values are used for all members of the Σ isotopic multiplet and their antipartners, and remain unchanged for all beam particles and target combinations. PYTHIA was used with its default set of parameters, and no attempt was made to change them to obtain better fits to our experimental data, since this would destroy the agreement with other experimental results (for a discussion of this point, see [4]). We included elastic and diffraction processes (PYTHIA option `MSEL=2`) and used the Lund string fragmentation algorithm, which is closer to the ansatz of the QGSM model than 'independent' or 'cluster' fragmentation.

Since PYTHIA can only deal with reactions on single nucleons, an extrapolation to the carbon and copper targets was made assuming $\sigma \propto A^{\alpha}$ with $\alpha = 2/3$. In Fig. 13–14 our differential cross sections $\mathrm{d}\sigma/\ \mathrm{d}\ x_F$ for the carbon target are compared with the PYTHIA and QGSM predictions.

The production of Σ^- hyperons by Σ^- at high x_F is better described by PYTHIA than by the QGSM, because the elastic contribution is included in PYTHIA only. If left out (option `MSEL=1`), the PYTHIA result coincides with the QGSM result. The role of elastic and soft diffraction processes is much less pronounced in Σ^+ production by Σ^-, and here the slopes obtained by PYTHIA and the QGSM model are in agreement with the observed slope.

As mentioned above, our data show essentially no difference in the production of Σ^-_{1385} by Σ^- and neutrons. This does not fit to the well-established leading particle effect, and both models, QGSM and PYTHIA, predict smaller cross sections for production by neutrons at high x_F.

On the other hand, we see a clear difference between Σ^+_{1385} production by Σ^- and neutrons. The QGSM tends to underestimate this effect.

The most significant, and even striking discrepancy between the theoretical estimations and the experimental results is observed in the production of Σ^+ and Σ^- hyperons by pions, where the observed x_F spectra are much harder than the calculated ones. This effect remains totally unexplained by models.

Finally, in the case of $\overline{\Sigma}^-$ production by Σ^-, the absense of common quarks in the initial hyperon and the final anti-hyperon results in an x_F spectrum much steeper than any x_F spectrum observed in Σ or Σ^* production. This effect is reproduced at least qualitatively by both models.

Acknowledgements. It is a pleasure to thank J. Zimmer and G. Konorova for their support in setting up and running the experiment. We are also indebted to the staff of the CERN Omega spectrometer group for their help and support, to the CERN EBS group for their work on the hyperon beam line and to the CERN accelerator group for their continuous efforts to provide good and stable beam conditions. We thank B.Kopeliovich for helpful discussions.

References

1. S.F.Biagi et al., Z. Phys. C **34**, 187 (1987)
2. T. Sjöstrand, Computer Phys. Comm. **82**, 74 (1994)
3. Yu.A.Alexandrov et al., Z. Phys. C **76**, 35 (1997)
4. Yu.A.Alexandrov et al., Eur.Phys.J. C **11**, 271 (1999)
5. A.B. Kaidalov, K.A. Ter-Martirosyan, Sov. J. Nucl. Phys. **39**, 1545 (1984,) A.I. Veselov, O.I. Piskunova, K.A. Ter-Martirosyan, Phys. Lett. B **158**, 175 (1985,) A.B. Kaidalov, O.I. Piskunova, Z. Phys. C **30**, 145 (1986,) A.B. Kaidalov, Sov. J. Nucl. Phys. **45**, 1450 (1987)
6. S.P. Baranov, Lebedev Institute of Physics report **42**, 1998
7. J. Badier et al., Phys. Rev. Lett. **39B**, 414 (1972)
8. B.Y.Oh et al., Nucl. Phys. B **49**, 13 (1972)
9. V.Blobel et al., Nucl. Phys. B **69**, 454 (1974)
10. V.Hungerbühler et al., Phys. Rev. D **12**, 1203 (1975); Nucl. Instr. and Meth. **115**, 221 (1974)
11. M. Bourquin et al., Nucl. Phys. B **153**, 13 (1979)
12. M.Bardadin-Otwinowska et al., Nucl. Phys. B **90**, 397 (1975)
13. H.Kichimi et al., Phys. Lett. **72B**, 411 (1978)
14. S.Erhan et al., Phys. Lett. **85B**, 447 (1979)
15. D.Bricket al., Phys. Rev. D **25**, 2248 (1982)
16. A.N.Aleev et al., Yad. Fiz. **44**, 661 (1986); Sov.J.Nucl.Phys. **44**, 429 (1986)
17. R.Sugahara et al., Nucl. Phys. B **156**, 237 (1979)
18. H.C.Fenker et al., Phys. Rev. D **30**, 872 (1984)
19. S.Mikocki et al., Phys. Rev. D **34**, 42 (1986)
20. M.Baubillier et al., Z. Physik C **23**, 213 (1984)
21. M.Baubillier et al., Nucl. Phys. B **148**, 18 (1979)
22. F.Bareiro et al., Nucl. Phys. B **126**, 319 (1977)
23. H.Grassler et al., Nucl. Phys. B **118**, 189 (1977)
24. M.Bardadin et al., Nucl. Phys. B **98**, 418 (1975)
25. S.F. Biagi et al., Z. Physik C **9**, 305 (1981)
26. S.F.Biagi et al., Z. Phys.C **31**, 33 (1986)
27. O.Schneider et al., Z. Phys. C **46**, 341 (1990)
28. Yu.A.Alexandrov et al., CERN-SL-97-60 EA and Nucl. Instr. Meth. A **408**, 359 (1998)
29. W. Beusch, CERN/SPSC/77-70
30. D.Acostaet al., Nucl. Instr. and Meth.A **308**, 481 (1991); A **305**, 55 (1991); A **302**, 36 (1991)
31. M.Beck et al., Nucl. Instr. and Meth.A **355**, 351. (1995) M.Beck, Ph.D. Thesis, Rupert-Karl-Universität, Heidelberg (1996)
32. M.Firebaugh et al., Phys. Rev. **172**, 172 (1968)
33. R.A.Ponte et al., Phys. Rev. B **12**, 2597 (1975)
34. B.R.Martinet al., Nucl. Phys. B **126**, 266 (1977); Nucl. Phys. B **126**, 285 (1977); Nucl. Phys. B **126**, 349 (1977)
35. H.Koiso et al., Nucl. Phys. A **433**, 619 (1985)
36. The Particle Data Group, Eur. J. Phys, C **3**, 1 (1998)
37. W.F.Baker et al., Phys. Lett. **51B**, 303 (1974)
38. R. Blankenbecler, S.J. Brodsky, Phys. Rev. D **10**, 2973 (1974)
39. W.M. Geist, Nucl. Phys. A**525**, 149c (1991)